

The effect of intermediate frequency on sheath dynamics in collisionless current driven triple frequency capacitive plasmas

S. Sharma,^{1,a)} S. K. Mishra,^{1,2} P. K. Kaw,¹ and M. M. Turner³

¹*Institute for Plasma Research (IPR), Gandhinagar, India*

²*ELI-ALPS, Szeged, Hungary*

³*National Centre for Plasma Science and Technology, Dublin City University, Dublin, Ireland*

(Received 20 September 2016; accepted 27 December 2016; published online 12 January 2017)

The Capacitively Coupled Plasma discharge featuring operation in current driven triple frequency configuration has analytically been investigated, and the outcome is verified by utilising the 1D3V particle-in-cell (PIC) simulation code. In this analysis, the role of middle frequency component of the applied signal has precisely been explored. The discharge parameters are seen to be sensitive to the ratio of the chosen middle frequency to lower and higher frequencies for fixed amplitudes of the three frequency components. On the basis of analysis and PIC simulation results, the middle frequency component is demonstrated to act as additional control over sheath potential, electron sheath heating, and ion energy distribution function (iedf) of the plasma discharge. For the electron sheath heating, effect of the middle frequency is seen to be pronounced as it approaches to the lower frequency component. On the other hand, for the iedf, the control is more sensitive as the middle frequency approaches towards the higher frequency. The PIC estimate for the electron sheath heating is found to be in reasonably good agreement with the analytical prediction based on the Kaganovich formulation. *Published by AIP Publishing.* [<http://dx.doi.org/10.1063/1.4973889>]

I. INTRODUCTION AND MOTIVATION

The efficacy of operating capacitively coupled plasma (CCP) discharges at low pressure (\sim mTorr) configuration makes it a promising tool (e.g., as a plasma source for etching and thin film deposition) for microelectronics industry in the fabrication of large scale integrated circuits.^{1–5} In material processing, uniform etching/deposition over the electrode and control over sheath plasma parameters, ion flux, and energy are essential.¹ In case of conventional CCP source, the discharge is driven by a single frequency source, and all these parameters are coupled to each other. Thus, it is not possible to individually control the various plasma discharge features in conventional CCP discharges.^{3–5} In contrast, the recent studies^{5–9} elucidate that such discrete control over plasma discharge features can be obtained by using non-harmonic, tailored, or multi frequency signals over discharge electrodes. This fact is further supported by numerous analytical works based on hydrodynamic modelling,^{10–13} simulation (fluid and particle-in-cell (PIC)) studies,^{14–16} and experimental campaigns.^{17–19}

Dual frequency (*df*-) CCP discharge, proposed by Goto *et al.*,^{20,21} is an example of controlled discharge operation where simultaneously operative high and low frequency RF signals are used to separately control the plasma density (ionization) and ion energy (bias voltage). Using the PIC Monte Carlo collision (PIC-MCC) simulation, Georgieva and Bogaerts²² demonstrated that the ion energy distribution function (iedf) gets broadened when the fundamental frequency (27 MHz) is used together with the low frequency source (1–2 MHz); the broadening is observed to be large in case of 1 MHz than that of 2 MHz. It is also noticed that the

average ion energy is driven by time averaged voltage across the sheath, which itself is sensitive to the applied signal voltage and frequency ratios. From the existing studies, it is known that in the high frequency regime (*say*), the system length may exceed the excitation wavelength and may lead to a distorted iedf, resulting in the non-uniformity near electrodes. For example, an increase in high frequency signal voltage leads to the shift of iedf towards higher energy and may damage the surface material. On the other hand, decrease in the low frequency signal voltage results in shifting of iedf towards lower energy and weakens the plasma etching rate.^{22–28} In recent studies,²⁹ it is proposed that distortion in energy extremes, which arises in *df*-CCP can be tackled (i.e., by controlling iedf) by introducing an intermediate frequency with *df*-CCP discharge configuration. Furthermore,^{23–26} non-sinusoidal signals (configured with multiple harmonics) and tailored waveforms have also been used for more efficient control of discharge operations (i.e., fine tuning of ion energy and ion flux and hence iedf). The applicability of such configurations is limited because of the coupling between applied multiple harmonics, which might lead to an asymmetric plasma response. A detailed analysis of merits and limitations of the use of non-sinusoidal waveforms in CCP discharges may be found in the elegant review by Lafluer.²⁷

In this paper, we would like to systematically discuss the stochastic heating and iedf control in the case of triple frequency CCP (tf-CCP). The effect of mid frequency insertion in tf-CCP has been illustrated by various numerical simulation techniques,^{29–32} but most of the analysis so far has been restricted to a homogeneous sheath modelling³³ and far from realistic sheath features. It is only recently that Rahman and Dewan³⁴ have considered the sheath inhomogeneity

^{a)}E-mail: sarvsarvesh@gmail.com

following Lieberman's³⁵ analysis. In particular, the sheath dynamics has been examined in terms of the instantaneous sheath position and mean potential. In the low pressure regime, collisionless heating of the electrons is the dominant mechanism of energy transport/deposition in the vicinity of the sheath. This heating primarily ensues as a consequence of mutual interaction between expanding/collapsing phase of the sheath in response to the applied oscillatory RF field.³⁶ This effect has been verified experimentally^{37,38} and by simulation techniques.^{45–50} In the present analysis, we intend to investigate the characteristic features of CCP discharge operating with the triple frequency source in the current driven mode. The current driven mode is chosen here because in the present analysis, we use the Lieberman³⁵ model as a standard approach and investigate how the use of multiple frequencies modifies these results. The current driven mode also simplifies the problem by artificially switching off the plasma series resonance effect, which can contribute significantly to electron heating in CCP discharges.^{1,35,40} We anticipate that in the tf-CCP case, scaling of average sheath potential and ion energy (etching rate) by adjusting the intermediate frequency should be possible. First, this has been examined by an analytical formulation, and after that, it is further verified with a self-consistent *1D-multiple port electrostatic particle in cell* (PIC) simulation code. The outcome may provide insight for designing the laboratory experiments and may also be helpful for industrial applications.^{39,42–44}

To get physical insight of the problem, we establish an analytical formulation for the CCP discharge operating in the low pressure collisionless regime with a triple frequency current driven signal. The algebraic form of the transient profile associated with the applied triple frequency current source can be written as

$$j(x) = [j_l \sin \omega_l t + j_m \sin(\omega_m t + \theta_m) + j_h \sin(\omega_h t + \theta_h)], \quad (1a)$$

$$\Rightarrow j(x) = j_l[\sin(\omega_l t) + c_{ml} \sin(\alpha \omega_l t + \theta_m) + c_{hl} \sin(\beta \omega_l t + \theta_h)] = j_l f_o, \quad (1b)$$

where j , $\omega (=2\pi f)$, and θ are the amplitude, frequency, and phase of the applied current source, respectively; the subscripts l , m , and h refer to lower, intermediate, and highest frequency components of applied signal, $\alpha = \omega_m/\omega_l$, $\beta = \omega_h/\omega_l$, $c_{ml} = j_m/j_l$, & $c_{hl} = j_h/j_l$ with $j_l = 4 \text{ A/m}^2$, $j_m = 20 \text{ A/m}^2$, $j_h = 40 \text{ A/m}^2$, and $f_l = 2 \text{ MHz}$, $f_m = 16 \text{ MHz}$, $f_h = 80 \text{ MHz}$; other simulation parameters are described in subsequent Section III. It should be noted here that experimental reactors operating in the low pressure regime are geometrically asymmetric,^{51–65} and thus, the current form may significantly differ from the algebraic form stated in Eq. (1). In fact, the use of multiple harmonic signals over electrodes causes electrical asymmetry and sets a finite dc field between the electrodes.^{2–4} Consequently, the sheath response modulates the iedf, which effectively reflects the ion flux and energy available for deposition. This asymmetry can be regulated up to a desired extent by adjusting the frequency and phase between externally applied signals which gives additional control over discharge confinement and relevant plasma

parameters. Nevertheless, concerning our prime emphasis in this paper on exploring the influence of the intermediate frequency in the CCP discharge and comparison with the well known analytical models,^{31,36} we confine our analysis to symmetric electrode system only.

The temporal profile of the applied signal in single frequency (sf), dual frequency (df), and triple frequency (tf) mode is illustrated in the figures (Fig. 2(a)). In simulation, the pulse train has been applied to the electrodes, and the system is left to evolve and attain steady state situation; the steady state features of the discharge parameters over a complete RF cycle have graphically been illustrated. The sheath dynamics in CCP discharge operating in the tf configuration eventually depends on the cumulative current profile modulated due to frequency manifestation of all the three signals; we follow the analysis by Lieberman³⁵ and Kaganovich *et al.*⁴⁰ to establish the expressions for sheath parameters and heating of electrons in Section II. Section III includes the description of the *1D-multiple port electrostatic* particle-in-cell (PIC) simulation code and parameters used for the computations. The physical interpretation and discussion of the numerical results based on the analysis have been given in Section IV. Finally, a summary of the outcome in Section V concludes the paper.

II. ANALYTICAL MODELLING: SHEATH STRUCTURE AND COLLISIONLESS SHEATH HEATING OF ELECTRONS

In this section, utilizing the formalism adopted by Lieberman³⁵ and Kaganovich *et al.*,⁴⁰ we derive the expressions for the sheath structure and consequent collisionless heating of the electrons in the proximity of the sheath region in a CCP discharge, driven by triple frequency setup. To get a clear idea about the conceptual features of the discharge, a schematic of *tf* configuration of the CCP discharge in the current driven mode (*similar to Ref. 33*) has been displayed in Fig. 1(a). Following Lieberman,³⁵ the *Poisson* equation for the instantaneous electric field (E) in the sheath region can be expressed as

$$\left(\frac{\partial E}{\partial x}\right) = \begin{cases} (e/\epsilon_0)n_i(x), & s(t) < x \\ = 0 & s(t) > x. \end{cases} \quad (2)$$

Here, $s(t)$ refers to the distance from the ion sheath edge (at $x = 0$) to the electron sheath edge, x is an arbitrary position in the sheath region, $n_i(x)$ is the axial ion density, ϵ_0 is the permittivity of free space, and e refers to the electronic charge (see Fig. 1(b), Ref. 17). Here, we have taken the simplified RF electron sheath model (step function) given by Lieberman³⁵ for analysis. In recent works (e.g., Brinkmann⁶⁵), by using a more sophisticated electron sheath model, the presence of significant electric field in the bulk-sheath transition region is visualized which in turn also perceived to contribute in electron sheath heating.^{66,67} However, concerning our motivation to explore the influence of intermediate frequency on discharge features, as the first step, we keep our case simple and use the Lieberman³⁵ and Kaganovich *et al.*⁴⁰ approach for the analysis. Manifesting the Poisson equation with number and energy conservation of ions in the sheath region, the equations

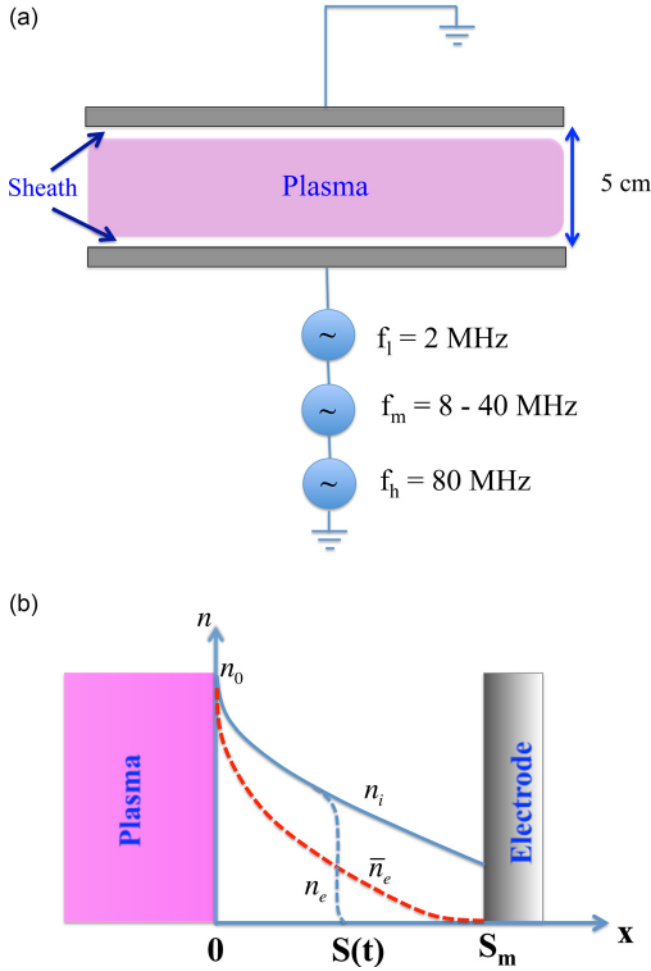


FIG. 1. (a) The schematic diagram of low pressure current driven Ar plasma discharge in the *tf*-mode. (b) The schematic diagram of high voltage single frequency capacitively coupled plasma sheath.

for the parameters governing the sheath structure, viz., for the mean electric field, electric potential, and electron/ ion density can be expressed as³⁵

$$(d\bar{E}/dx) = (e/\epsilon_0)[n_i(x) - \bar{n}_e(x)], \quad (3)$$

$$(d\bar{\varphi}/dx) = -\bar{E}, \quad (4)$$

$$\bar{n}_e(x) = [1 - (\gamma/\pi)]n_i(x), \quad (5)$$

and

$$n_i(x) = n_0(1 - 2\bar{\varphi}/T_e)^{-1/2}, \quad (6)$$

where E , φ , and n_e/n_i are the electric field, potential, and electron/ ion density, respectively; n_0 is the mean density of electrons/ions in bulk (ion sheath edge), and γ refers to the arbitrary phase associated with position x in the sheath region; the bar on these quantities corresponds to the time average values over one *RF* cycle. The motion of the instantaneous electron sheath, which is driven by applied current signal, can be written as

$$\begin{aligned} n_i(x)u_s &= n_i(x)(ds/dt) = j(x) \\ &= [j_i \sin \omega t + j_m \sin(\omega_m t + \theta_m) + j_h \sin(\omega_h t + \theta_h)], \end{aligned} \quad (7)$$

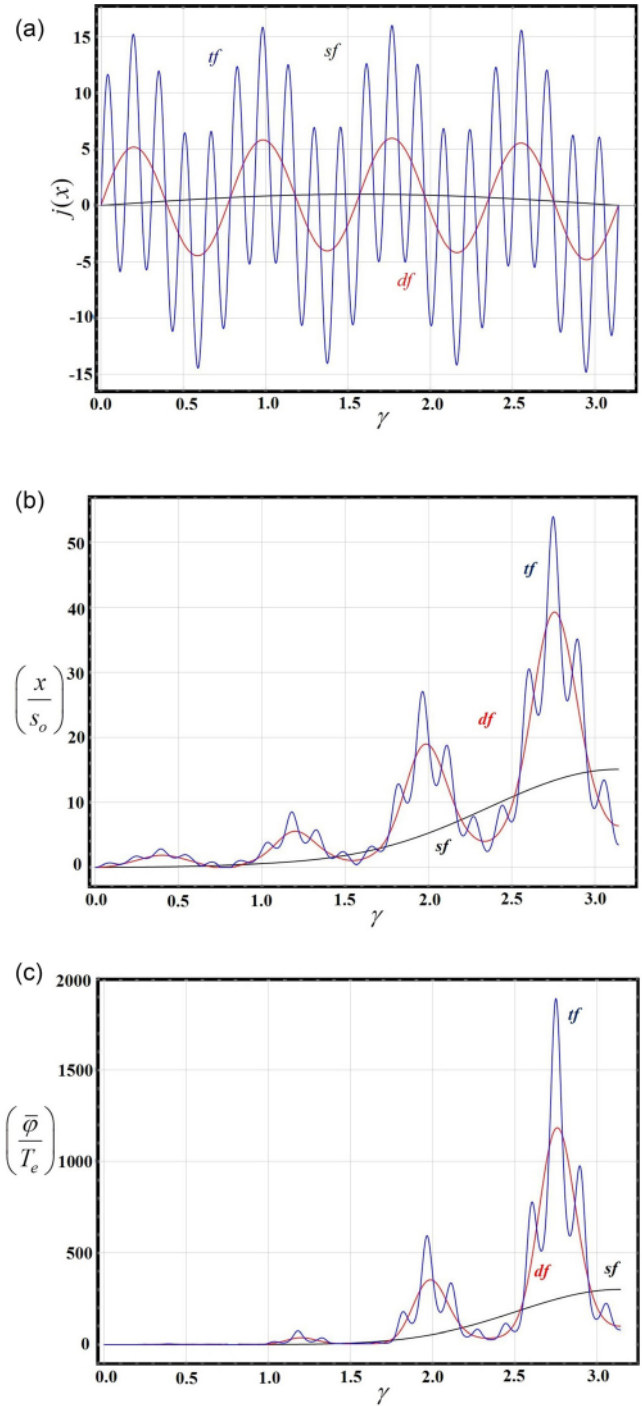


FIG. 2. (a) The time profile of the applied current signal over discharge electrode in *sf*, *df*, and *tf* modes for standard set of parameters stated in the text. (b) The normalized position (x) of *RF* electron sheath as a function of phase (γ) in different discharge operating *sf*, *df*, and *tf* modes for standard set of parameters stated in the text. (c) Corresponding normalized mean electric potential ($\bar{\varphi}$) as a function of phase (γ) in different discharge operating *sf*, *df*, and *tf* modes for standard set of parameters stated in the text.

where u_s is the velocity of the electron sheath edge.

Following the algebraic steps given in Ref. 35, one can combine the space and time integrations of Eqs. (2) and (7), respectively, to obtain the instantaneous electric field as

$$\begin{aligned}
E(x, \omega t) &= \frac{e}{\varepsilon_0} \int_0^x n_i(\zeta) d\zeta - \frac{1}{\varepsilon_0} \left[\frac{j_l}{\omega_l} (1 - \cos \omega_l t) \right. \\
&\quad + \frac{j_m}{\omega_m} [\cos \theta_m - \cos(\omega_m t + \theta_m)] \\
&\quad \left. + \frac{j_h}{\omega_h} [\cos \theta_h - \cos(\omega_h t + \theta_h)] \right] \quad s(t) < x, \\
&= 0 \quad s(t) > x. \quad (8)
\end{aligned}$$

The time average electric field (\bar{E}) at any position x in the sheath can be obtained by integrating Eq. (8) over an rf -period within limits $\gamma = \pm \omega_l t$ and can be written as

$$\begin{aligned}
\bar{E}(x) &= -(d\bar{\varphi}/dx) = (1/2\pi) \int_{-\gamma}^{\gamma} E(x, \omega t) d(\omega t) \\
\Rightarrow &= \left(\frac{e\gamma}{\varepsilon_0 \pi} \right) \int_0^x n_i(\zeta) d\zeta - (1/\pi \varepsilon_0 \omega_l) \left[j_l(\gamma - \sin \gamma) \right. \\
&\quad + (j_m/\alpha^2)(\alpha\gamma - \sin \alpha\gamma) \cos \theta_m \\
&\quad \left. + (j_h/\beta^2)(\beta\gamma - \sin \beta\gamma) \cos \theta_h \right]. \quad (9)
\end{aligned}$$

Using Eq. (9) in limiting conditions, viz., $x = s$ and $\omega t = \gamma$ at any particular x in the sheath region, one obtains

$$\begin{aligned}
\bar{E}(x) &= -\left(\frac{d\bar{\varphi}}{dx} \right) = \left(\frac{j_l}{\pi \varepsilon_0 \omega_l} \right) \left[(\sin \gamma - \gamma \cos \gamma) \right. \\
&\quad + \left(\frac{c_{ml}}{\alpha^2} \right) [\cos \theta_m \sin \alpha\gamma - \alpha\gamma \cos(\alpha\gamma + \theta_m)] \\
&\quad \left. + \left(\frac{c_{hl}}{\beta^2} \right) [\cos \theta_h \sin \beta\gamma - \beta\gamma \cos(\beta\gamma + \theta_h)] \right] \\
&= \left(\frac{j_l}{\pi \varepsilon_0 \omega_l} \right) g_o. \quad (10)
\end{aligned}$$

Substituting the mean ion density (Eq. (6)) in the sheath dynamics equation (Eq. (7)), with $x = s$ and $\omega t = \gamma$, one thus obtains

$$\begin{aligned}
\left(1 - \frac{2\bar{\varphi}}{T_e} \right)^{1/2} \left(\frac{d\gamma}{dx} \right) &= (1/s_o) [\sin \gamma + c_{ml} \sin(\alpha\gamma + \theta_m) \\
&\quad + c_{hl} \sin(\beta\gamma + \theta_h)]^{-1} = (1/s_a f_o), \quad (11)
\end{aligned}$$

with $s_o (= j_l/n_o e \omega_l)$. The set of equations, viz., Eqs. (10) and (11), yields a self-consistent description of the RF sheath and phase evolution. Combining Eqs. (10) and (11) and integrating with appropriate boundary conditions, viz., $\bar{\varphi} = 0$ at $\gamma = 0$, one can easily be solved to get the time averaged potential structure, as follows:

$$\begin{aligned}
\frac{d\bar{\varphi}}{(1 - 2\bar{\varphi}/T_e)^{1/2}} &= -\left(\frac{s_o j_l}{\pi \varepsilon_0 \omega_l} \right) f_o g_o d\gamma \Rightarrow \left(1 - \frac{2\bar{\varphi}}{T_e} \right)^{1/2} \\
&= 1 + H \int f_o g_o d\gamma, \quad (12)
\end{aligned}$$

where $H (= s_o^2/\pi \lambda_d^2)$ and $\lambda_d [= (\varepsilon_0 T_e/en_o)^{1/2}]$ are the Debye length. This equation also refers to the ion density and can be expressed by using it (Eq. (12)) with Eq. (6) as follows:

$$n_i(x) = n_o \left(1 - \frac{2\bar{\varphi}}{T_e} \right)^{-1/2} = n_o \left[1 + H \int f_o g_o d\gamma \right]^{-1}. \quad (13)$$

Substituting for $\bar{\varphi}$ from Eq. (12) in Eq. (11) and integrating it again with initial boundary conditions $\gamma = 0$ at $x = 0$, one can write

$$(x/s_o) = \int f_o [1 + H \int f_o g_o d\gamma] d\gamma. \quad (14)$$

The above set of derived equations (Eqs. (10)–(14)) describes the time averaged sheath evolution of the discharge parameters self-consistently and can be solved numerically for any particular case/choice of parameters. It is also verified that the present analysis is consistent with the available analytical expression for fundamental sinusoidal signal by putting $j_m = j_h = 0$. The oscillatory motion of the sheath invokes the potential and field structures, which eventually characterizes iedf. The consistent nonlinear evolution of the sheath motion and discharge parameters, viz., mean electric field (\bar{E}) and mean electric potential ($\bar{\varphi}$), corresponding to the triple frequency setup has been illustrated as a function of phase (γ).

The plasma electrons interacting with oscillating electron sheath lose energy in its collapsing phase while some of the electrons gain energy in the expanding sheath; effectively in an rf -period, electrons gain a finite energy. However, in literature, the presence of field reversal during the collapsing phase of sheath (for hydrogen, neon, and electronegative plasmas) has been reported, which may contribute the additional electron heating.^{68–74} This effect is ignored in the present analysis. Using the kinetic approach for the current driven mode in the case of single frequency discharge, this average energy gain by electrons in the collisionless regime has been estimated by Lieberman.³⁵ Following the approach similar to that of Lieberman,³⁵ the sheath heating can be written as

$$S_L = m_e u_e \langle (u_s - v_o) n_s u_s \rangle_\gamma \Rightarrow m_e u_e j_l \langle (u_s - v_o) f_o \rangle_\gamma, \quad (15)$$

where $u_s = (ds/dt) = u_a f_o [1 + H \int f_o g_o d\gamma]$ is the instant sheath edge velocity and $v_o (= u_a f_o)$ refers to the time varying oscillatory velocity of the electrons (at ion sheath edge) under the influence of applied rf current with $u_o = (j_l/n_o)$. This refers to $(u_s - v_o) \sim u_a f_o H \int f_o g_o d\gamma$, and Eq. (15) can be written as

$$S_L = m_e n_o u_e u_o^2 \left\langle f_o^2 H \int f_o g_o d\gamma \right\rangle = S_o \left\langle f_o^2 H \int f_o g_o d\gamma \right\rangle_\gamma. \quad (16)$$

However, this estimate for sheath heating by the Lieberman³⁵ treatment ignores the influence of the applied electric field on bulk electrons. This assumption violates the current conservation condition at the electron sheath edge.^{20,24} This fact was taken into account by Kaganovich *et al.*⁴⁰ in their analysis, and the formulation established that Lieberman expression overestimates the sheath heating for low H values in case of sf current profile. Following the Kaganovich kinetic treatment, the modified expression for sheath heating can be written as follows:

$$S_K = m_e n_o u_e u_o^2 \langle (u_s - v_o)^2 (n_i/n_o) \rangle_\gamma$$

$$= S_o \left\langle f_o^2 H^2 \left[\int f_o g_o d\gamma \right]^2 \left[1 + H \int f_o g_o d\gamma \right]^{-1} \right\rangle_\gamma. \quad (17)$$

It is also verified that the electron sheath heating expressions (i.e., Eqs. (16) and (17)) with $j_m = j_h = 0$ readily reduces to the known expressions for the fundamental sf sinusoidal signal, derived in the previous analyses.^{35,40,41} It is also verified that the electron sheath heating given by the Kaganovich formulation approaches asymptotically at higher H to the Lieberman estimate.

III. SIMULATION SCHEME AND PARAMETERS

We have simulated the current driven triple frequency discharge by using the 1D3V electrostatic PIC code for the argon plasma in a low pressure regime where the discharge is primarily sustained by sheath heating of electrons. The code has been developed by the group of Professor Miles Turner at *Dublin City University* and has been utilized in numerous recent studies;^{75–79} a detailed description about the simulation approach can be seen in Refs. 45 and 46. The simulation takes account of all the possible interaction processes between the particles (viz., elastic/inelastic/charge exchange/ionization) via manifesting the Particle-in-Cell (PIC)^{45,46} and Monte Carlo collision (MCC)^{47,48} schemes together; these have been utilized to estimate the self-consistent plasma discharge features. The accuracy, stability, and resolution of the simulation have been taken care of by appropriate choice of step size of time and space, which are taken to be smaller than the plasma frequency and the Debye length. The discharge system is composed of mutually parallel coupled electrodes of infinite dimension, which can be operated in both, viz., current and voltage driven modes; in this particular analysis, we have used it in the current driven mode. In order to simulate the present analysis, the electrode gap of 5 cm filled with argon (*Ar*) gas at low pressure (5 mTorr) has been considered. In order to compare the simulation results with the analytical treatment, the boundary walls (electrodes) are considered perfectly absorptive for the plasma particles, and the secondary electron emission from the electrodes is ignored. The simulation has been carried out for the following standard set of discharge plasma parameters, and the effect of individual parameter has been examined keeping the other parameters constant:

$j_l = 4\text{A/m}^2$, $j_m = 20\text{A/m}^2$, $j_h = 40\text{A/m}^2$, $f_l = 2\text{MHz}$, $f_m = 16\text{MHz}$, $f_h = 80\text{MHz}$, $\phi_l = \phi_m = \phi_h = 0$, $c_{ml} = 5$, $c_{hl} = 10$, $\alpha = 8$, $\beta = 40$, $T_{eo} = 17406\text{K}$, $T_{io} = T_g = 300\text{K}$, and $p_g \approx 5\text{mTorr}$; T_{eo} and $T_{io}(T_g)$ are the initial electron and ion (gas) temperature, while p_g refers the gas pressure. Here, we vary middle frequency, i.e., f_m , and we keep other simulation parameters constant.

A train of current driven pulse (as given in Eq. (1)) has been applied for longer period of time in order to achieve the steady state plasma discharge, and the numerous plasma parameters in an rf -cycle have been displayed as outcome. We have evaluated the electron sheath heating and $iedf$ of the discharge in the triple frequency current driven mode;

in-particular, the effect of intermediate frequency (f_m) component on numerous physical parameters, keeping rest the parameters same, and the results are discussed in Section IV.

IV. NUMERICAL RESULTS AND DISCUSSION

It is well understood that the applied rf -source over the electrode causes an instantaneous oscillatory electric field response to the plasma electrons, prominently in the proximity of the electrodes. The applied field significantly diminishes within few Debye scale lengths while moving from the electrodes to the centre of discharge (i.e., the sheath region (as $E_x \propto e^{-x/\lambda_d}$)). A much weaker electric field exists inside the bulk or pre-sheath region, and the plasma density self-consistently decays from the centre of discharge to electrodes. In general, in an RF cycle the electrons interacting with expanding sheath get kicks, and depending on the interaction of the phase with the electron sheath edge, electrons either gain or lose energy. On the other hand, electrons lose its energy during collapsing phase of the sheath. However, over an RF cycle, there is a net gain in the electron energy. When multiple frequency signals are applied to the electrodes, the instantaneous movement of electrons depend on the superposition of constituent current signals; in particular, to the resulting electric field, whose amplitude, following Maxwell equations, varies proportional to the current magnitude and inversely proportional to the frequency component (i.e., $E_{rf} \propto j_{rf}/f_{rf}$). For instance, if one chose the peak current in all three cases, viz., sf , df , and tf modes constant, the sheath features are sensitive to the choice of the frequencies. It is well understood and stated before that in the df -CCP discharge, lower and higher frequency components control the features of $iedf$ and plasma ionization, respectively; the inclusion of intermediate frequency intuitively stimulates that particular aspect, which is closer to it due to the significant mutual frequency overlap. For example, one should anticipate large sheath potential drop (additional control over $iedf$) in case of $f_m \rightarrow f_l$ while larger plasma density as $f_m \rightarrow f_h$. This characteristic also replicates in collisionless sheath heating with multiple signals where it is anticipated to decrease with increasing the higher frequency components.²³ First, we illustrate the numerical results for the sheath parameters and electron sheath heating, corresponding to the analytical formulation made in Section II. The simulation results based on PIC has been discussed in the consequent Subsection IV B.

A. Numerical results with analytical formulation

The set of Fig. 2 demonstrates the steady state self-consistent nonlinear discharge evolution as a function of phase (γ) by the inclusion of higher frequency component. The computations correspond to the standard set of parameters mentioned in Section III. Fig. 2(a) reflects the current form in the three cases, viz., when the discharge is operated in sf , df , and tf modes. As anticipated, the powered electrode is driven by superposition of multiple current signals. The sheath oscillation (span, x) and corresponding evolution of the mean sheath potential ($\bar{\phi}$) in the expanding phase (i.e.,

$0 \leq \gamma \leq \pi$) of the oscillation have been illustrated in Figs. 2(b) and 2(c), respectively. Symmetrical behaviour is anticipated in collapsing phase, i.e., $\pi \leq \gamma \leq 2\pi$. The sheath span (x) and mean sheath potential ($\bar{\varphi}$) are seen to be larger in the *tf* driven discharge than that in the case of *sf* mode for the chosen set of data; the $\bar{\varphi}$ variation also reciprocates the evolution of the mean electric field (\bar{E}). The collisionless capacitive electron sheath heating based on the Kaganovich formulation in these three different operating modes has been displayed in Fig. 3(a) as a function of the parameter H . The sheath heating is seen to be largest in case of the *tf* operating mode. This is primarily a consequence of a large mean sheath potential (Fig. 2(c)). The Kaganovich formulation is noticed to approach the *Lieberman* estimate with the inclusion of additional frequency components and increasing values of parameter H ; this nature has been showed in Fig. 3(b) for the given set of parameters. Next, we consider the case of *tf* operated mode for our further computation and try to explore the role of middle frequency component in the CCP discharge.

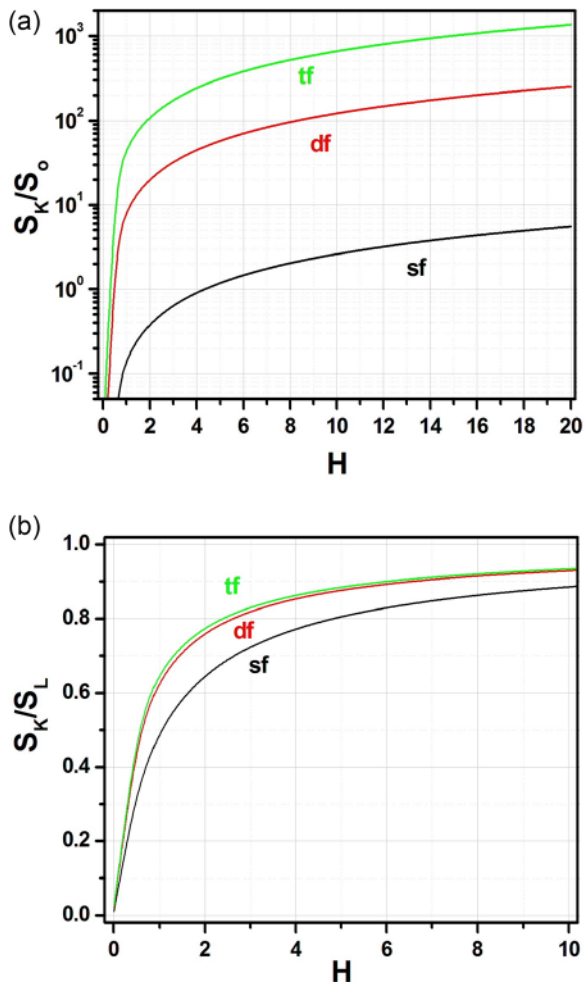


FIG. 3. (a) Average electron sheath heating (Kaganovich estimate) as a function of parameter H for the discharge operating in *sf*, *df*, and *tf* modes for standard set of parameters stated in the text. (b) The ratio of electron sheath heating estimates based on Kaganovich and Lieberman formulation as a function of parameter H for the discharge operating in *sf*, *df*, and *tf* modes for standard set of parameters stated in the text.

The evolution (x) of electron sheath by varying the middle frequency in the *tf* discharge configuration has been illustrated in Fig. 4(a), and as anticipated, the span is noticed to increase as the middle frequency approaches to lower

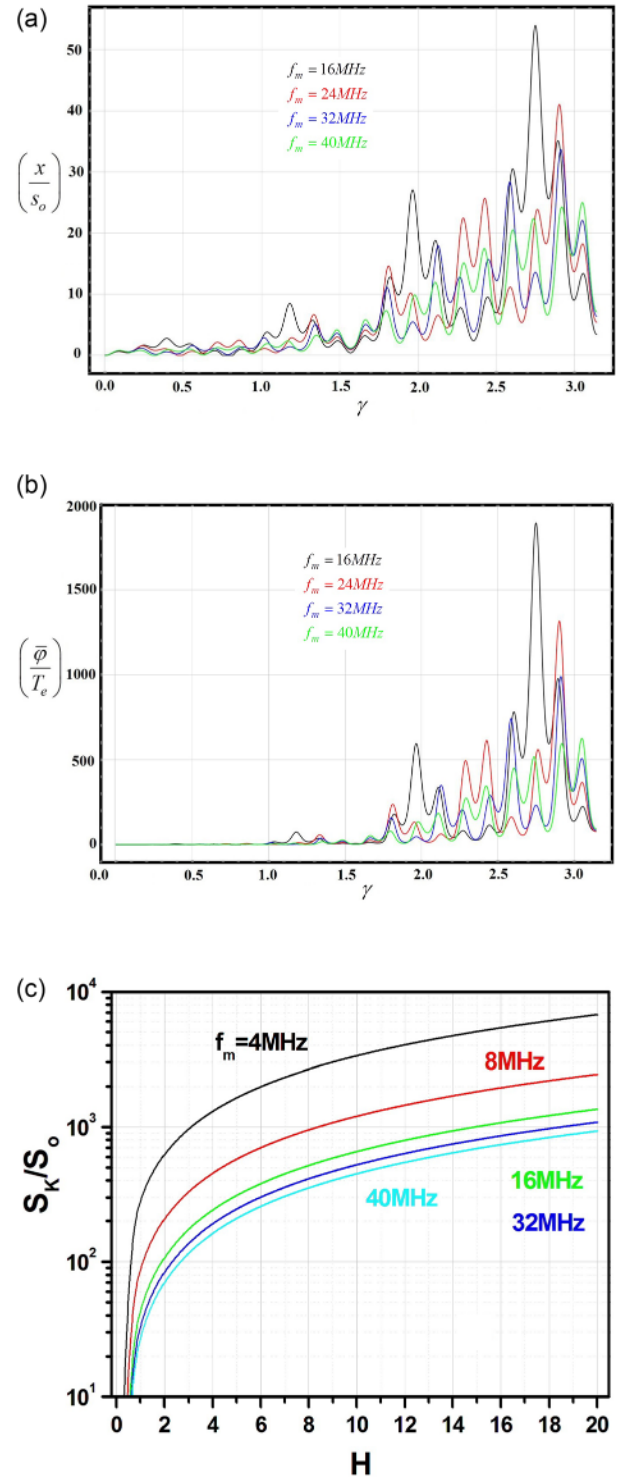


FIG. 4. (a) Normalized position (x) of *RF* electron sheath as a function of phase (γ) in the discharge operating in the *tf* mode for different values of f_m corresponding to standard set of parameters stated in the text. (b) Normalized mean electric potential ($\bar{\varphi}$) as a function of phase (γ) in the discharge operating in the *tf* mode for different values of f_m corresponding to (a). (c) Kaganovich estimate of electron sheath heating (Kaganovich estimate) as a function of parameter H in the discharge operating in the *tf* mode for different values of f_m corresponding to (a).

frequency (~ 2 MHz). Corresponding variation of f_m on the discharge sheath potential has been displayed in Fig. 4(b). It is found that the sheath potential fluctuates at higher magnitude as f_m approaches to lower frequency f_l . In particular, the analytically calculated sheath potential drops significantly at $f_m \sim 40$ MHz compared to ~ 16 MHz (Fig. 4(b)). This average sheath potential physically determines the ion energy distribution function (iedf), responsible for etching and film deposition in material processing using CCP discharges. The decrease in the sheath potential with increasing f_m may cause the absence of high energy ions and possess low energy particles in the proximity of electrode. The mean energy gained (Kaganovich estimate) by electrons due to oscillatory sheath in the collisionless regime has been displayed in Fig. 4(c) and follows the trend similar to Figs. 4(a) and 4(b) as the heating is noticed to increase as $f_m \rightarrow f_l$. This nature can be attributed to the effects due to the appropriate superposition and weaker destructive interference between the frequency components of applied current signals, as intermediate frequency approaches the lowest frequency.

B. PIC results for CCP discharge with *tf* configuration

The PIC simulation has been conducted using the 1D3V electrostatic code for the set of data given in Section III, and the role of middle frequency component in *tf* configuration has been explored. In simulation results, the powered electrode is located at 0 cm, and grounded electrode is at 5 cm. The time averaged electron (dashed line) and ion (solid line) density profile in the steady state of the plasma discharge have been illustrated in Fig. 5. The peak density in the curve shows a peculiar phenomenon in which it rises and falls as the middle frequency is increased. On the other hand, the total number of ions in the discharge seems to monotonically go up with the increase in the middle frequency f_m . This may be attributed to an optimization in the number of the electrons/ions in the discharge volume for a particular intermediate frequency ($f_m \sim 20$ MHz). The increase of electrons/ions in the discharge volume with increasing f_m is primarily due to the enhancement of effective modulated frequency in the *tf* mode. As a consequence, the sheath width (span) is

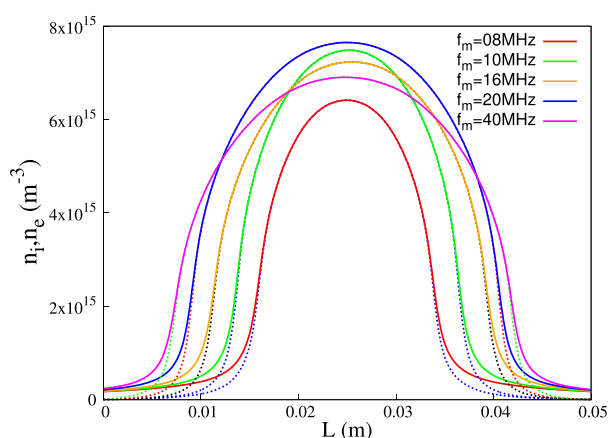


FIG. 5. Space evolution of the time average plasma density (n_e, n_i) in the discharge operating in the *tf* mode for different values of f_m and standard set of parameters stated in text.

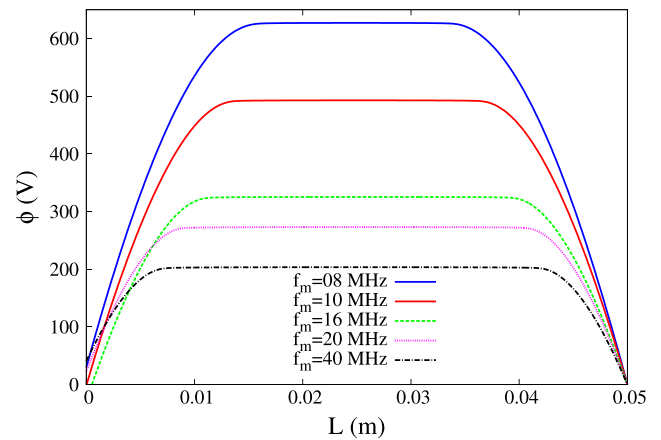


FIG. 6. Space evolution of the time mean electric potential ($\bar{\phi}$) in the discharge operating in the *tf* mode for different values of f_m corresponding to Fig. 5.

discerned to decrease and is in qualitative agreement with the analytical assessment (Fig. 4(a)). This can be understood in terms of increase in plasma shielding with the increasing density. Theory predicts the average sheath span (in cm) of $\sim 1.78, 1.51, 1.34, 1.24,$ and 0.79 for $f_m = 8$ MHz, 10 MHz, 16 MHz, 20 MHz, and 40 MHz, respectively, which is in reasonable agreement with the *PIC* results (verified from density profile in Fig. 5). The axial profile of mean plasma potential of the discharge has been displayed in Fig. 6 where it is seen to be large when the middle frequency f_m is close to lower frequency. This fact is also consistent with our analytical prediction (Fig. 4(b)). The effect of f_m on iedf at the powered electrode (0 cm) is primarily governed by potential drop over the sheath and has been described in Fig. 7. It is noticed that the presence of high energy ions decreases as f_m approaches to the high frequency component. At $f_m = 40$ MHz, the energy of ions is significantly reduced (~ 300 eV) compared to $f_m = 08$ MHz (~ 800 eV). This may be attributed to decrease in the sheath potential with increasing f_m and consequently a control over the production of highly energetic ions.

In collisionless case, as a consequence of the sheath oscillation, the interacting electrons in collapsing and expanding

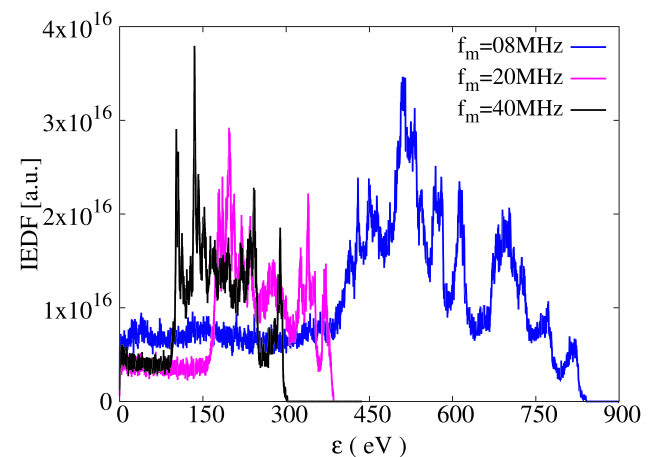


FIG. 7. Corresponding ion energy distribution function (iedf) at the powered electrode ($x=0$ cm) in CCP discharge operating in the *tf* mode for different values of f_m corresponding to Fig. 5.

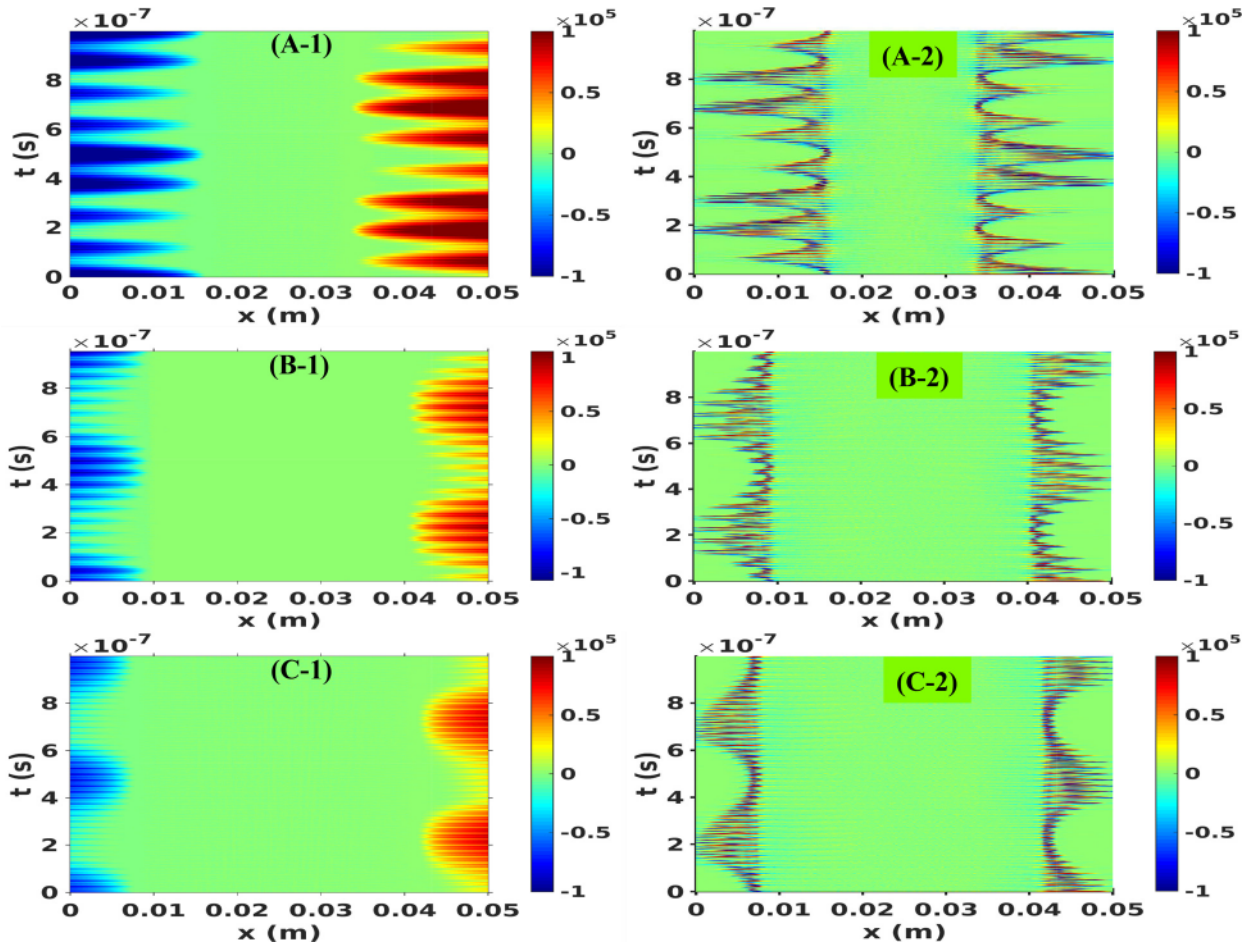


FIG. 8. The spatio-temporal profile of the electric field (E) and corresponding electron sheath heating ($\langle J.E \rangle$) in the discharge operating in the tf mode for different of f_m values viz., 8 MHz ((A-1),(A-2)), 20 MHz ((B-1),(B-2)), and 40 MHz ((C-1),(C-2)).

phases effectively gain a finite positive energy in an rf-cycle. This results in the collisionless heating of electrons in the vicinity of sheath. The spatiotemporal profile of the electric field and the sheath heating for $f_m = 8$ MHz, 20 MHz, and 40 MHz have been displayed in Fig. 8 for last two rf cycles. The interplay of sheath dynamics and its consequent increase in sheath heating by reducing the middle frequency are clearly visible in this figure. The time averaged electron sheath heating corresponding to different values of f_m is shown in Fig. 9. In this discharge profile, the collisionless electron sheath heating peaks at some point in the proximity of the sheath edge; this can be understood in terms of mutual competitive phenomena of decreasing local electric field and increasing plasma density ($J.E \propto n_e E^2$) in sheath. The electron sheath heating is seen to acquire double peaks at smaller f_m values; this may correspond to the peaks occurring in the sheath potential (Fig. 4) in an RF cycle, which drives the electron heating effectively in the sheath. It should be noted that the net heating (S_{stoc}) is composed of contributions from both, viz., applied RF (S_{rf}) current signal and the dc sheath part S_{dc} (i.e., *floating sheath*). The dc floating sheath eventually refers to the negative heating (S_{dc}) in the proximity of the electrode, which means the plasma near the electrode becomes colder. In simulation, the rf electron sheath heating (S_{rf}) has been obtained by dropping the dc contribution (S_{dc}) from the net collisionless heating (S_{sh}). An estimate of the time average

(averaged over 100 RF cycles) sheath heating of the electrons ($S_{rf} = S_{sh} - S_{dc}$) using PIC simulation operating in tf mode for different f_m has been depicted in Fig. 10 (solid blue dots with line). It clearly demonstrates that the sheath heating is sensitive to the frequency ratios (i.e., f_m) in tf -mode of discharge operation. The points refer to the analytical prediction of the electron sheath heating as a function of f_m

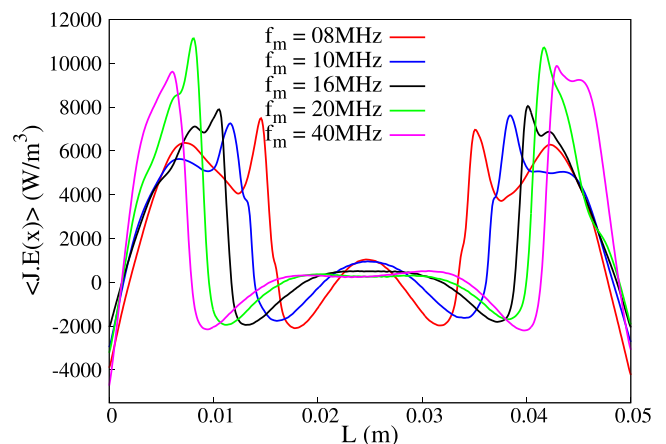


FIG. 9. Space evolution of the time average electron sheath heating ($\langle J.E \rangle$) in the discharge operating in the tf mode for different values of f_m corresponding to Fig. 5.

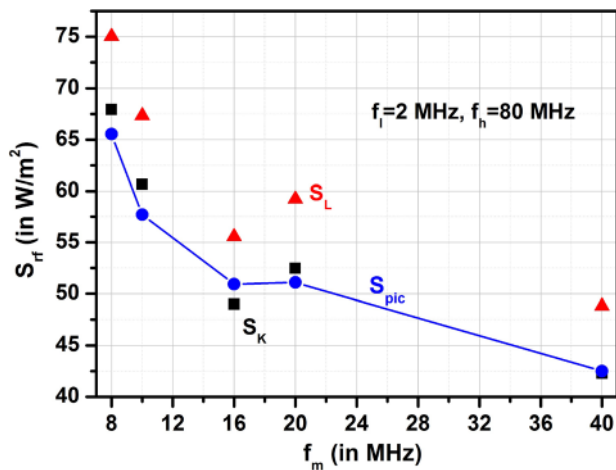


FIG. 10. Average electron sheath heating (S_{stoc}) as a function of middle frequency component (f_m); the red (triangle) and black (square) dots refer to Lieberman and Kaganovich estimate while the blue dots with line correspond to PIC results.

corresponding to the data set used for PIC simulation; red (triangle) and black (square) solid points refer to Lieberman (S_L , Eq. (16)) and Kaganovich (S_K , Eq. (17)) estimates, respectively. The PIC estimates are observed to be in reasonable agreement with the Kaganovich formulation. The analytical (Figs. 3 and 4) and the PIC simulation (Figs. 6–8) estimates reveal an important feature that the sheath dynamics, ion energy, and electron sheath heating can be controlled by scaling the intermediate frequency in tf -configuration of CCP discharge. Further, it should be noted that the outcomes of the analysis are strictly relevant to the system operating in the collisionless regime.

V. SUMMARY

In summary, an analytical model (based on sf sheath modelling given by Lieberman³⁵ and Kaganovich *et al.*⁴⁰) for stochastic heating in tf current driven CCP discharge has been developed. It is observed that the stochastic heating is dependent on the intermediate frequency of the applied RF signal. The heating estimated by the analytical model has been further verified with the help of the 1D3V electrostatic PIC code and found in reasonable agreement with simulation results. It is also observed that the ion energy distribution function (iedf) at the electrode can be controlled by tuning the intermediate frequency. The maximum energy of ions arriving at the electrodes reduces when the middle frequency approaches the higher frequency. This is because the potential across sheath is modified by tuning the middle frequency. It allows a control over power deposition at the electrode in CCP discharges. This is of relevance to the etching/ deposition processes in numerous material processing applications in micro-nano fabrications.

ACKNOWLEDGMENTS

This work was supported by Department of Science and Technology (DST), Government of India via Projects GITA/DST/TWN/P-56/2014, DST-JC Bose Fellowship, and YOS Professor PKK 92-14.

- ¹M. Lieberman and A. J. Lichtenberg, *Principles of Plasma Discharges and Materials Processing* (Wiley, NJ, 2005).
- ²B. G. Heil, U. Czarnetzki, R. P. Brinkmann, and T. Mussenbrock, *J. Phys. D: Appl. Phys.* **41**(16), 165202 (2008).
- ³J. Schulze, E. Schungel, and U. Czarnetzki, *J. Phys. D: Appl. Phys.* **42**, 092005 (2009).
- ⁴J. Schulze, E. Schungel, Z. Donko, and U. Czarnetzki, *Plasma Sources Sci. Technol.* **20**, 015017 (2011).
- ⁵Z. Donko, J. Schulze, P. Hartmann, I. Korolev, U. Czarnetzki, and E. Schungel, *Appl. Phys. Lett.* **97**, 081501 (2010).
- ⁶E. Schungel, J. Schulze, Z. Donko, and U. Czarnetzki, *Phys. Plasmas* **18**, 013503 (2011).
- ⁷Z. Donko, *Plasma Sources Sci. Technol.* **20**, 024001 (2011).
- ⁸T. Lafleur and J. P. Booth, *J. Phys. D: Appl. Phys.* **45**, 395203 (2012).
- ⁹D. J. Coumou, D. H. Clark, T. Kummerer, M. Hopkins, D. Sullivan, and S. Shanon, *IEEE Trans. Plasma Sci.* **42**, 1880 (2014).
- ¹⁰L. Spitzer, *Physics of Fully Ionized Gases*, 2nd edition (John Wiley, 1962).
- ¹¹M. Olevanov, O. Proshina, T. Rakhimova, and D. Voloshin, *Phys. Rev. E* **78**, 026404 (2008).
- ¹²W. C. Chen, X. M. Zhu, S. Zhang, and Y. K. Pu, *Appl. Phys. Lett.* **94**, 211503 (2009).
- ¹³D. Israel and K.-U. Riemann, *J. Appl. Phys.* **99**, 093303 (2006).
- ¹⁴J. K. Lee, O. V. Manuilenko, N. Yu. Babaeva, H. C. Kim, and J. W. Shon, *Plasma Sources Sci. Technol.* **14**, 89 (2005).
- ¹⁵Z. Zhou, R. Linghu, M. Deng, and D. Xiong, *J. Appl. Phys.* **112**, 063306 (2012).
- ¹⁶T. Lafleur, R. W. Boswell, and J. P. Booth, *Appl. Phys. Lett.* **100**, 194101 (2012).
- ¹⁷T. V. Rakhimova, O. V. Braginsky, V. V. Ivanov, A. S. Kovalev, D. V. Lopaev, Y. A. Mankelevich, M. A. Olevanov, O. V. Proshina, A. T. Rakhimov, A. N. Vasilieva, and D. G. Voloshin, *IEEE Trans. Plasma Sci.* **35**, 1229 (2007).
- ¹⁸T. Lafleur, P. A. Delattre, E. Johnson, and J. P. Booth, *Appl. Phys. Lett.* **101**, 124104 (2012).
- ¹⁹P. A. Delattre, T. Lafleur, E. Johnson, and J. P. Booth, *J. Phys. D: Appl. Phys.* **46**, 235201 (2013).
- ²⁰H. H. Goto, H. D. Lowe, and T. Ohmi, *J. Vac. Sci. Technol.*, **A 10**, 3048 (1992).
- ²¹H. H. Goto, H. D. Lowe, and T. Ohmi, *IEEE Trans. Semicond. Manuf.* **6**, 58 (1993).
- ²²V. Georgieva and A. Bogaerts, *J. Appl. Phys.* **98**, 023308 (2005).
- ²³S. Sharma, S. K. Mishra, P. K. Kaw, A. Das, N. Sirse, and M. M. Turner, *Plasma Sources Sci. Technol.* **24**, 025037 (2015).
- ²⁴M. M. Patterson, H. Y. Chu, and A. E. Wendt, *Plasma Sources Sci. Technol.* **16**, 257 (2007).
- ²⁵T. Baloniak, R. Reuter, and A. von Keudell, *J. Phys. D: Appl. Phys.* **43**, 335201 (2010).
- ²⁶E. Schüngel, Z. Donkó, P. Hartmann, A. Derzsi, I. Korolev, and J. Schulze, *Plasma Sources Sci. Technol.* **24**, 045013 (2015).
- ²⁷T. Lafleur, *Plasma Sources Sci. Technol.* **25**, 013001 (2016).
- ²⁸H. C. Kim, J. K. Lee, and J. W. Shon, *Phys. Plasmas* **10**, 4545 (2003).
- ²⁹C. F. Alan Wu, M. A. Lieberman, and J. P. Verboncoeur, *J. Appl. Phys.* **101**, 056105 (2007).
- ³⁰H. C. Kim and J. K. Lee, *Phys. Rev. Lett.* **93**, 085003 (2004).
- ³¹H. C. Kim, F. Iza, S. S. Yang, M. Radmilovic-Radjenovic, and J. K. Lee, *J. Phys. D: Appl. Phys.* **38**, R283 (2005).
- ³²G. Y. Park, S. J. You, F. Iza, and J. K. Lee, *Phys. Rev. Lett.* **98**, 085003 (2007).
- ³³S. H. Lee, P. K. Tiwari, and J. K. Lee, *Plasma Sources Sci. Technol.* **18**, 025024 (2009).
- ³⁴M. T. Rahman and M. N. A. Dewan, *Plasma Sci. Technol.* **17**, 141 (2015).
- ³⁵M. A. Lieberman, *IEEE Trans. Plasma Sci.* **16**, 638 (1988).
- ³⁶S. Sharma, "Investigation of ion and electron kinetic phenomena in capacitively coupled radio-frequency plasma sheaths: A simulation study," Ph.D. thesis (Dublin City University, 2013).
- ³⁷O. A. Popov and V. A. Godyak, *J. Appl. Phys.* **57**, 53 (1985).
- ³⁸V. A. Godyak and R. B. Piejak, *Phys. Rev. Lett.* **65**, 996 (1990).
- ³⁹I. D. Kaganovich, V. I. Kolobov, and L. D. Tsensin, *Appl. Phys. Lett.* **69**, 3818 (1996).
- ⁴⁰I. D. Kaganovich, O. V. Polomarov, and C. E. Theodosiou, *IEEE Trans. Plasma Sci.* **34**, 696 (2006).
- ⁴¹E. Kawamura, M. A. Lieberman, and A. J. Lichtenberg, *Phys. Plasmas* **13**, 053506 (2006).

- ⁴²S. Sharma and M. M. Turner, *J. Phys. D: Appl. Phys.* **46**, 285203 (2013).
- ⁴³S. Sharma, S. K. Mishra, and P. K. Kaw, *Phys. Plasmas* **21**, 073511 (2014).
- ⁴⁴S. Sharma, S. K. Mishra, P. K. Kaw, M. M. Turner, and S. K. Karkari, *Contrib. Plasma Phys.* **55**(4), 331 (2015).
- ⁴⁵J. P. Verboncoeur, *Plasma Phys. Controlled Fusion* **47**, A231 (2005).
- ⁴⁶M. M. Turner, A. Derzsi, Z. Donkó, D. Eremin, and S. J. Kelly, *Phys. Plasmas* **20**, 013507 (2013).
- ⁴⁷C. K. Birdsall, *IEEE Trans. Plasma Sci.* **19**, 65 (1991).
- ⁴⁸R. W. Hockney and J. W. Eastwood, *Computer Simulation Using Particles* (Adam Hilger, Bristol, 1988).
- ⁴⁹S. Sharma and M. M. Turner, *Plasma Sources Sci. Technol.* **22**(3), 035014 (2013).
- ⁵⁰S. Sharma and M. M. Turner, *Phys. Plasmas* **20**, 073507 (2013).
- ⁵¹J. Schulze, B. G. Heil, D. Luggenhölscher, R. P. Brinkmann, and U. Czarnetzki, *J. Phys. D: Appl. Phys.* **41**, 195212 (2008).
- ⁵²J. Schulze, B. G. Heil, D. Luggenhölscher, T. Mussenbrock, R. P. Brinkmann, and U. Czarnetzki, *J. Phys. D: Appl. Phys.* **41**, 042003 (2008).
- ⁵³B. M. Annaratone, V. P. T. Ku, and J. E. Allen, *J. Appl. Phys.* **77**, 5455 (1995).
- ⁵⁴V. P. T. Ku, B. M. Annaratone, and J. E. Allen, *J. Appl. Phys.* **84**, 6536 (1998).
- ⁵⁵W. D. Qiu, K. J. Bowers, and C. K. Birdsall, *Plasma Sources Sci. Technol.* **12**, 57 (2003).
- ⁵⁶U. Czarnetzki, T. Mussenbrock, and R. P. Brinkmann, *Phys. Plasmas* **13**, 123503 (2006).
- ⁵⁷T. Mussenbrock and R. P. Brinkmann, *Appl. Phys. Lett.* **88**, 151503 (2006).
- ⁵⁸T. Mussenbrock, D. Zeigler, and R. P. Brinkmann, *Phys. Plasmas* **13**, 083501 (2006).
- ⁵⁹T. Mussenbrock and R. P. Brinkmann, *Plasma Sources Sci. Technol.* **16**, 377 (2007).
- ⁶⁰L. Tonks, *Phys. Rev.* **37**, 1458 (1931).
- ⁶¹L. Tonks, *Phys. Rev.* **38**, 1219 (1931).
- ⁶²A. Dattner, *Phys. Rev. Lett.* **10**, 205 (1963).
- ⁶³J. V. Parker, J. C. Nickel, and R. W. Gould, *Phys. Fluids* **7**, 1489 (1964).
- ⁶⁴J. Taillet, *Am. J. Phys.* **37**, 423 (1969).
- ⁶⁵R. P. Brinkmann, *Plasma Sources Sci. Technol.* **24**, 064002 (2015).
- ⁶⁶R. P. Brinkmann, *Plasma Sources Sci. Technol.* **25**, 014001 (2016).
- ⁶⁷J. Schulze, Z. Donko, A. Derzsi, I. Korolov, and E. Schuengel, *Plasma Sources Sci. Technol.* **24**, 015019 (2015).
- ⁶⁸D. O'Connell, T. Gans, A. Meige, P. Awakowicz, and R. W. Boswell, *IEEE Trans. Plasma Sci.* **36**, 1382 (2008).
- ⁶⁹A. Meige, D. O'Connell, T. Gans, and R. W. Boswell, *IEEE Trans. Plasma Sci.* **36**, 1384 (2008).
- ⁷⁰T. Gans, C. C. Lin, V. Schulz-von der Gathen, and H. F. Dobebe, *Phys. Rev. A* **67**, 012707 (2003).
- ⁷¹M. M. Turner and M. B. Hopkins, *Phys. Rev. Lett.* **69**, 3511 (1992).
- ⁷²U. Czarnetzki, D. Luggenhölscher, and H. F. Dobebe, *Plasma Sources Sci. Technol.* **8**, 230 (1999).
- ⁷³R. A. Gottscho, *Phys. Rev. A* **36**, 2233 (1987).
- ⁷⁴A. H. Sato and M. A. Lieberman, *J. Appl. Phys.* **68**, 6117 (1990).
- ⁷⁵M. M. Turner, *Plasma Sources Sci. Technol.* **22**, 055001 (2013).
- ⁷⁶P. C. Boyle, A. R. Ellingboe, and M. M. Turner, *Plasma Sources Sci. Technol.* **13**, 493 (2004).
- ⁷⁷J. Conway, S. Kechkar, N. O'Connor, C. Gaman, M. M. Turner, and S. Daniels, *Plasma Sources Sci. Technol.* **22**, 045004 (2013).
- ⁷⁸L. Lauro-Taroni, M. M. Turner, and N. StJ. Braithwaite, *J. Phys. D: Appl. Phys.* **37**, 2216 (2004).
- ⁷⁹M. M. Turner, A. W. Hutchinson, R. A. Doyle, and M. B. Hopkins, *Phys. Rev. Lett.* **76**, 2069 (1996).